Hindawi
Journal of Chemistry
Volume 2019, Article ID 4260153, 14 pages
https://doi.org/10.1155/2019/4260153

Research Article

Carbon Nanotubes: Synthesis via Chemical Vapour Deposition without Hydrogen, Surface Modification, and Application

Nguyen Duc Vu Quyen, Dinh Quang Khieu, Tran Ngoc Tuyen, Dang Xuan Tin, and Bui Thi Hoang Diem

Department of Chemistry, University of Sciences, Hue University, 77 Nguyen Hue Str., Hue, Vietnam

Correspondence should be addressed to Nguyen Duc Vu Quyen; ndvquyen@hueuni.edu.vn

Received 21 January 2019; Revised 23 April 2019; Accepted 19 June 2019; Published 2 July 2019

Academic Editor: Cristina Femoni

The present study describes the growth of carbon nanotubes (CNTs) from liquefied petroleum gas (LPG) on an Fe_2O_3/Al_2O_3 precatalyst via a chemical vapour deposition (CVD) process without hydrogen. The obtained multiwalled CNTs exhibit a less-defective structure with an identical external diameter of tubes of around 50 nm. The growth mechanism of CNTs suggests that the Fe_2O_3/Al_2O_3 precatalyst is reduced to Fe/Al_2O_3 during the synthesis process using the products of LPG decomposition, and the tip-growth mechanism is suggested. The resulting CNTs are surface-modified with potassium permanganate in the acid medium and used as an adsorbent for copper from aqueous solutions. The Langmuir and Freundlich isotherm models are employed to evaluate the adsorption data, and the maximum adsorption capacity of Cu(II) is 163.7 $mg \cdot g^{-1}$.

1. Introduction

In 1991, carbon nanotubes (CNTs) were detected by Iijima (Japan) in the carbon soot of graphite electrodes during arc discharge. The tubes were formed by the rolling of graphene sheets (single layer of carbon atoms (C-sp^2) arranged in a hexagonal lattice) [1]. With a cylindrical structure and nanometer-sized diameter, CNTs have been extensively known for many outstanding physical properties such as extraordinary mechanical durability, very high electrical and thermal conductivity, or optical properties [1], and because of this, the market for CNTs is heating up by many scientists in the world. In 1994, Guo et al. synthesized CNTs from carbonaceous gas using laser ablation [2]. Despite high-quality nanotubes, both of the arc discharge and the laser ablation were not popularly used due to very high temperature (around 3000°C) resulting in complicated equipment and low efficiency. The third method used by Endo et al. in 1993 for synthesizing CNTs [3] is chemical vapour deposition (CVD). Until present, CVD has been a widespread method due to low growth temperature (less than 1000°C), simple furnace, high efficiency, and high purity of the product [4].

During the chemical vapour deposition, the carbon feedstock in the form of hydrocarbon was decomposed at a specified temperature into carbon gas deposited on transition metal catalysts such as Fe, Co, or Ni. Numerous studies report that the synthesis of CNTs using pure hydrocarbon sources such as CH_4 [5], C_2H_2 [6], ethanol [7], or CO [8] is usually expensive because of the complex purification process. This results in high price of the obtained CNTs. Meanwhile, the price of natural carbon feedstock such as natural gas or liquefied petroleum gas (LPG) is much lower than that of pure hydrocarbons. Due to this advantage, LPG is popularly employed for the growth of CNTs by many scientists [9–12]. The growth of CNTs takes place when the amount of carbon in the solid solution with metal exceeds the saturation state [13, 14]. Therefore, in all previous studies, the metal oxide precatalyst that diffuses on the substrate (such as silica, alumina, or zeolite) has to be

reduced into metal by hydrogen before the decomposition of hydrocarbon [15–19]. This flow of hydrogen is maintained to prevent the obtained CNTs from oxidation until the synthesis terminates. The utilization of a large amount of hydrogen at high temperature for a long time not only raises the price of CNTs but also increases the danger during the operation of the furnace. As a result, the fabrication of CNTs must be carefully controlled. There is a little amount of research that recommends the fabrication of CNTs on the catalyst of Co and Ni without hydrogen [9, 20]. For that reason, the synthesis of CNTs without hydrogen is of considerable interest.

Heavy metal contamination in water is now an exigent problem for humans. Long-term exposure to toxic heavy metals can have carcinogenic effects on the central and peripheral nervous system and the circulatory system. The issue of "Lead and Copper Rule" in 1991 by the United State Environmental Protection Agency limits the concentration of lead and copper allowed in public drinking water at the consumer's tap [21] and stresses on the popularity and seriousness of these two heavy metals. Copper poisoning can cause stomach and intestinal distress, liver or kidney damage, and complications of Wilson's disease in genetically predisposed people. Therefore, the removal of copper from water is an essential study. Regarding the removal of Cu(II) with CNTs, many studies conducted so far have shown comparatively low values of maximum Cu(II) adsorption capacity [22–28]. The carbon nanotubes are known as an excellent adsorbent for heavy metals [29–32]. However, in the aqueous solution, the sorption ability is reduced because of the weak dispersion of CNTs caused by their noble nature. The adsorption behaviour of CNTs might be remarkably enhanced by surface modification. This modification using HNO_3, H_2SO_4, $KMnO_4$ H_2O_2, or NaClO increases the effective surface area of CNTs [33–35].

In the present study, CNTs are successfully synthesized from LPG via the CVD method using an Fe_2O_3/Al_2O_3 precatalyst without an initial flow of hydrogen. Nitrogen is used to create a noble medium to prevent the oxidation of CNTs. The mechanism of CNT growth is addressed. The obtained CNTs are modified using potassium permanganate and used as an adsorbent for copper from aqueous solutions.

2. Experimental

2.1. Materials

2.1.1. Preparation of Precatalyst. The precatalyst Fe_2O_3/Al_2O_3 with 25.9% of Fe_2O_3 (w/w) was prepared from $Fe(NO_3)_3{\cdot}9H_2O$ (Daejung, Korea) and Al_2O_3 (Daejung, Korea). Briefly, 50 mL of 0.35 M·$Fe(NO_3)_3$ solution was prepared and then added dropwise onto a 4 g-Al_2O_3 thin layer. The mixture was dried at room temperature for 10 hours and then at 100°C for 24 hours before calcination and at 500°C for 3 hours to completely pyrolyse $Fe(NO_3)_3$ to Fe_2O_3. The obtained red-brown precatalyst was ground and directly employed for the synthesis of CNTs. The SEM image of Fe_2O_3/Al_2O_3 precatalyst (Figure 1) exhibits uniform sphere particles with a size from 50 to 70 nm.

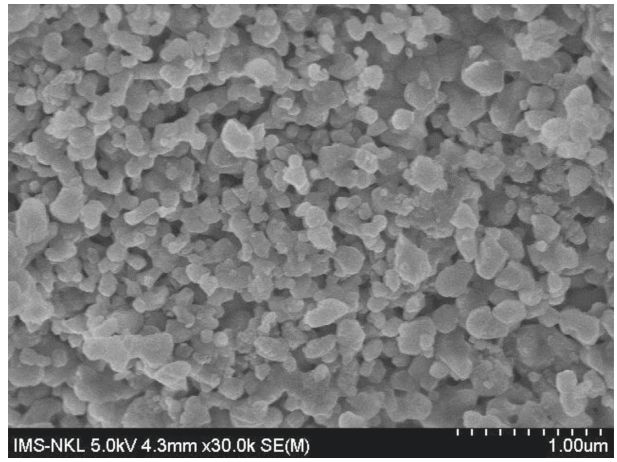

Figure 1: SEM image of Fe_2O_3/Al_2O_3 precatalyst.

2.1.2. Growth of Carbon Nanotubes. CNTs were synthesized from LPG (Dung Quoc oil refinery, Quang Ngai, Vietnam) via CVD using the Fe_2O_3/Al_2O_3 precatalyst. The temperature of the furnace is automatically controlled. A small ceramic boat containing 0.4 g of the Fe_2O_3/Al_2O_3 precatalyst was placed in the centre of the furnace. 60 mL·min^{-1} of nitrogen gas was blown through the furnace during the process. The furnace was heated to the growth temperature at 800°C. At this temperature, 100 mL·min^{-1} of LPG was blown into the furnace for 2 hours for CNTs to be grown up. The furnace was then cooled down to room temperature under the nitrogen flow. The product containing CNTs and Fe/Al_2O_3 catalyst was collected from the boat.

2.1.3. Surface Modification of Carbon Nanotubes. A quantity of 0.25 g of the resulting CNTs was ultrasonically suspended in 25 mL of a solution containing 0.1 M·$KMnO_4$ (Merck) and 0.5 M·H_2SO_4 (Merck) at 40°C for 2 hours. The surface-modified CNTs were separated, washed with deionized water until neutral, and dried at 80°C until constant weight. The suitable conditions of modification were determined on the basis of Cu(II) adsorption capacity. The concentration of Cu(II) was determined using atomic absorption spectrometry on Analyst 800 device (PerkinElmer, America).

2.2. Methods

2.2.1. Characterization of Materials. The crystal phase of the obtained CNTs was determined using X-ray diffraction (XRD) (RINT2000/PC, Rigaku, Japan) with $\lambda_{CuK\alpha} = 1.54$ Å. The elemental composition of CNTs was obtained from the energy-dispersive X-ray spectrum (EDS) (Hitachi S4800, Japan). The morphology of CNTs was observed using scanning electron microscopy (SEM) and scanning transmission electron microscopy (STEM) (Hitachi S4800, Japan). The STEM-EDS and HAADF-STEM (high-angle annular dark field) studies were used to determine the elemental composition of catalyst particles located inside the tubes. The SAED (selected area electron diffraction) and FFT (fast Fourier transform) measurements on the HR-TEM

(high-resolution transmission electron microscopy) device (Chemistem, Germany) were used to determine the lattice parameters of the material. The BET surface area of CNTs was analysed using N_2 adsorption and desorption on the BELSORP-mini device (Japan).

2.2.2. Adsorption Studies. All the working solutions of Cu(II) were further diluted from the stock solution containing 1000 mg·L^{-1}·Cu(II) (Merck).

The maximum Cu(II) adsorption capacity (q_m) of the surface-modified CNTs was determined on the basis of isothermal data. The samples including surface-modified CNTs and 50 mL of Cu(II) solution with the amount of Cu(II) ranging from 10 to 60 mg·L^{-1} were stirred at 30°C for 80 min. Here, the amount of surface-modified CNTs was fixed at 0.2 g·L^{-1}. The equilibrium amount of Cu(II) in the solution was determined after the adsorption. The adsorption capacity of Cu(II) was calculated according to the following equation:

$$q_e = \frac{C_0 - C_e}{m} \cdot V, \quad (1)$$

where q_e is the Cu(II) adsorption capacity; C_0 and C_e are the Cu(II) concentrations before and after adsorption, respectively; m is the mass of the surface-modified CNTs; and V is the volume of the Cu(II) solution.

3. Results and Discussion

3.1. Characterization of the Material. As can be seen, the XRD pattern of the synthesized product shown in Figure 2(a) exhibits characteristic peaks at 26.22° and 42.92° corresponding to the (002) and (100) diffraction planes of hexagonal graphite (JCPDS card files, No 41–1487), respectively [36]. Cao et al. [37] also confirm that these peaks are used to demonstrate the carbon crystal phase. This result proves that CNTs are the main product of the synthesis.

The EDS spectrum of CNTs (Figure 2(b)) reveals that the main composition of the product is carbon with a high-intensity peak at around 2.5 kV accounting for 91.24% of carbon. The low peaks of O, Al, and Fe observed with small weight percents are induced by Fe_2O_3/Al_2O_3 precatalyst.

The morphology of the synthesized CNTs is observed in the SEM images (Figure 3) and the STEM images (Figure 4). It is obvious that practically all tubes are long, less defective, and uniform. Some small particles appear on the tube, referring the remaining of the catalyst. The tube structure of CNTs is evidenced from the STEM images of the sample (Figure 4). The internal and external tube diameter is 15.2 ± 1.2 nm and 50 ± 2.3 nm ($n = 50$), respectively. The material might be multiwalled CNTs because the tube wall is relatively thick (16-17 nm).

The Russian Doll model [38] is recommended to describe the arrangement of graphene layers. High-magnification STEM images of CNTs (Figure 5) show that the wall of CNTs is thick and include many graphene layers arranged in concentric cylinders.

The synthesized CNTs exhibit a BET specific surface area of about 134 m^2·g^{-1}. The N_2 adsorption and desorption isotherms (Figure 6) are of type II according to the IUPAC classification, which is assigned to the multilayer adsorption of a macroporous material.

Before surface modification, the catalyst of Fe/Al_2O_3 in the product was removed with HCl·0.1 M. The modification causes several changes in bare CNTs. The EDS spectrum of bare CNTs shows that the material comprises only carbon, while the surface-modified CNTs exhibit some oxygen and manganese in the material (Figure 7). The absence of Fe and Al in the bare sample might be because the Fe/Al_2O_3 catalyst is removed by washing with HCl. The amount of oxygen demonstrates the presence of the functional groups containing oxygen appearing on the surface of CNTs. The small amount of manganese might be the product of $KMnO_4$ reduction.

The presence of functional groups on the CNTs was studied using FT-IR spectroscopy (Figure 8). The absorption bands assigned to –OH groups of carboxylic acid, alcohol, and water appear at around 3442 and 2920 cm^{-1}. Similarly, the band showing the presence of C=O groups in –COOH appears at around 1627 cm^{-1}. Wang et al. [22], Li et al. [25], and Moosa et al. [30] found similar characteristic bands for the surface-modified CNTs. The weak peak at the wavenumber of around 1550 cm^{-1} might be the evidence of C=C groups in the graphite structure.

Figures 9 and 10 show the SEM and TEM images of CNTs before and after surface modification. Generally, the tube structure remains after oxidization with $KMnO_4$. However, if we look closely into the microstructure of bare CNTs, we can see the tubes break resulting in shorter structures after modification. This is also observed in the Raman spectra (Figure 11). The D band (D-disorder) located at 1319 cm^{-1} shows the amorphous carbon and structural defects; the graphite structures are proved by the G band (G-graphite) at 1567 cm^{-1}. The G′ band at 2642 cm^{-1} is an overtone of the D band. The density of defects in the CNT structure could be estimated using the ratio of integrated intensities of the D and G bands (I_D/I_G). The larger the value of the I_D/I_G and $I_D/I_{G'}$ ratios, the higher would be the defect density [39]. The value of I_D/I_G for the surface-modified CNTs is 1.97, larger than that for bare CNTs (1.76), indicating some defects in the CNT structure.

The specific surface area of surface-modified CNTs measured using the BET method is 178 m^2·g^{-1}, larger than that of bare CNTs (134 m^2·g^{-1}). The rupture of CNTs indicates the formation of defects, i.e., the increase of the amount of pentagon and heptagon defects, resulting in the increase of the surface area [40].

3.2. Growth Mechanism of CNTs. The most commonly accepted growth mechanism of CNTs via the catalytic CVD method was postulated by Baker in the early 1970s [41], Yan et al. [42], Kumar and Ando [43], and Tessonnier and Su [44]. According to this mechanism, the hydrocarbon gas decomposes on the front-exposed surfaces of the metal particles to release hydrogen and the

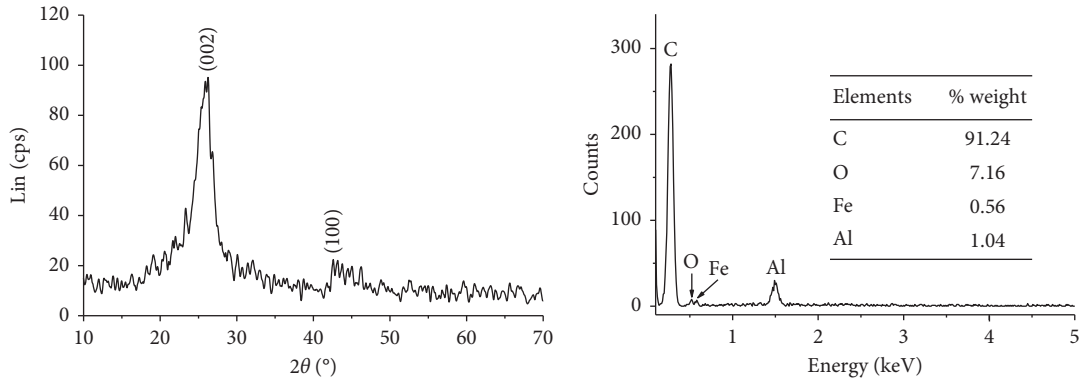

Figure 2: XRD (a) and EDS (b) studies of synthesized product sample.

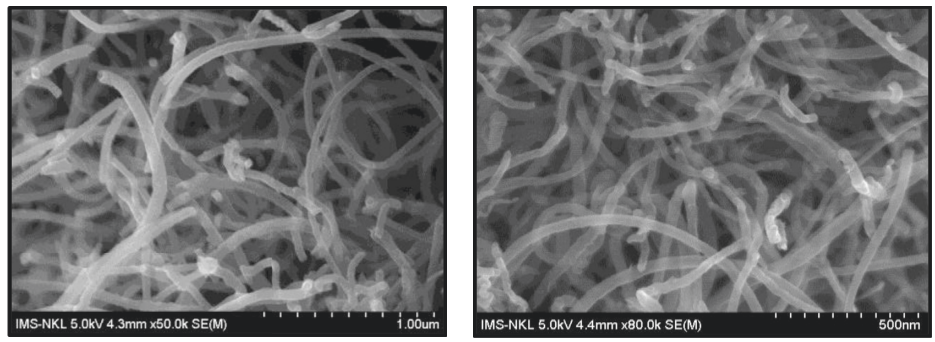

Figure 3: SEM images of synthesized product sample.

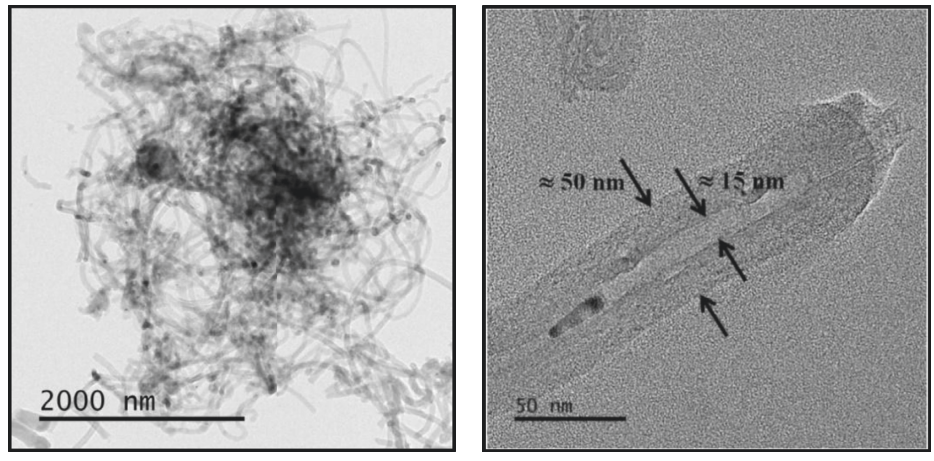

Figure 4: STEM images of synthesized product sample.

carbon gas dissolves in the metal particles. Since the solubility of carbon in the metal particle is temperature dependent, the precipitation of excess carbon will occur at the colder zone behind the particle, thus allowing the solid filament to grow with the same diameter as the width of the catalyst particles. Before the growth of CNTs, the precatalyst, which is metal oxide particles (such as Fe_2O_3 diffused on Al_2O_3 carrier), must be reduced to metal particles (Fe diffused on Al_2O_3) by hydrogen. This is one of the important periods in the synthesis of CNTs.

The present study skips this period and directly uses Fe_2O_3/Al_2O_3 as a precatalyst to synthesize CNTs. The mechanism of CNT growth is demonstrated from some extra analyses. Some dark particles observed inside the

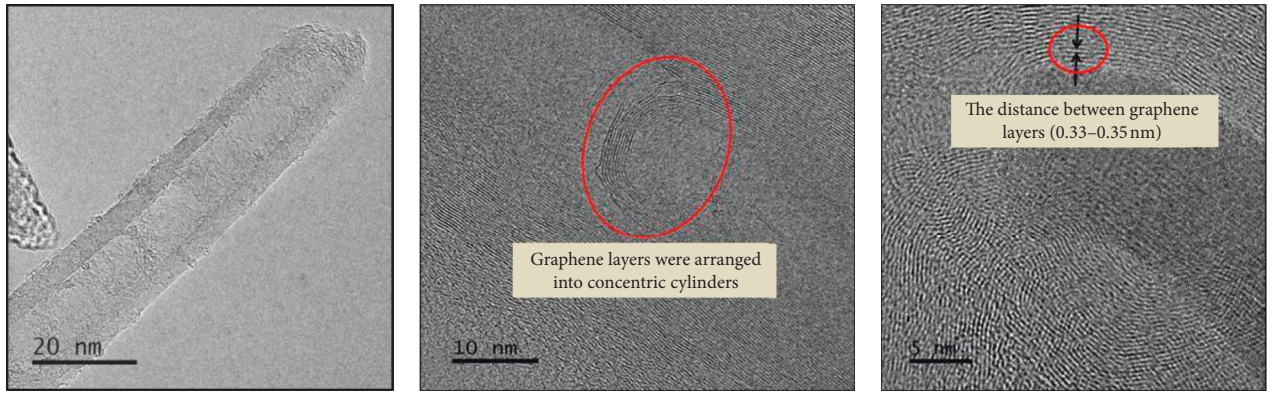

Figure 5: High-magnification STEM images of the CNT sample.

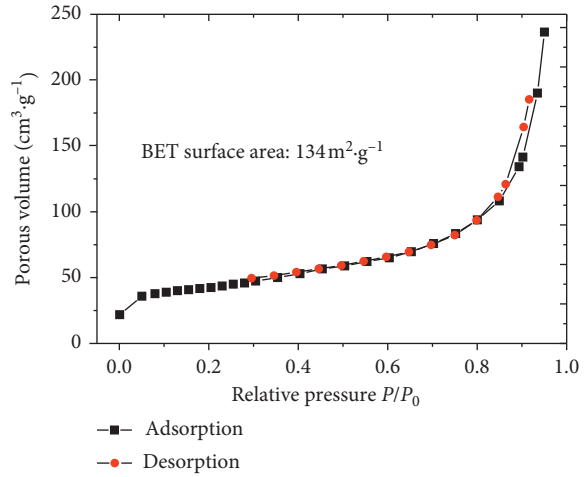

Figure 6: N_2 adsorption and desorption isotherms of the CNT sample.

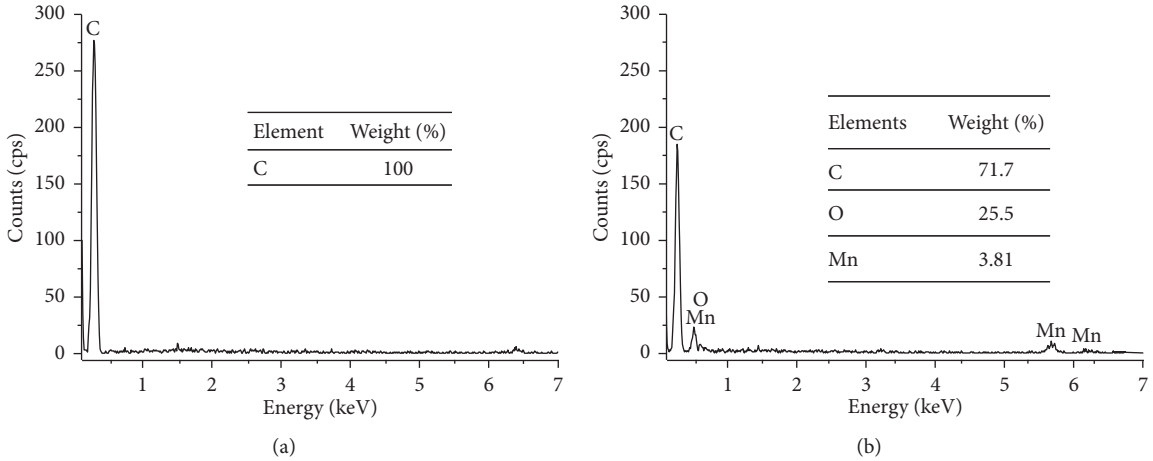

Figure 7: EDS analyses of bare CNTs (a) and surface-modified CNTs (b).

tubes on the STEM image of the CNT sample (Figure 4) might be nanoparticles of α-Fe.

Figure 12 shows that the signals of carbon, iron, aluminium, and oxygen atoms are expressed with different colours including red, blue, light-green, and Berlin blue, respectively. The appearance of dense signals indicates a high concentration of atoms. Figure 12(b) shows that in the observed field, the concentration of carbon is high. Iron

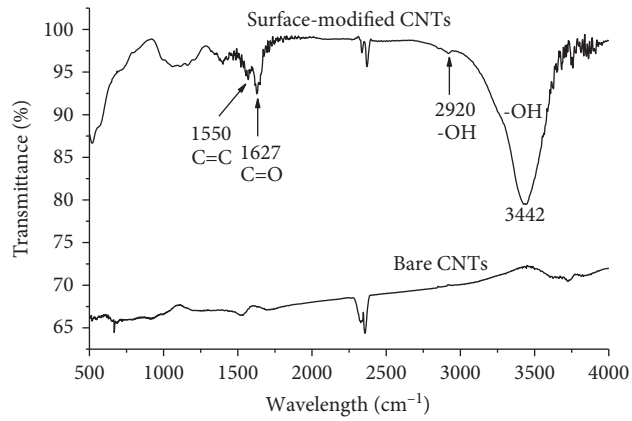

Figure 8: FT-IR spectra of bare CNTs and surface-modified CNTs.

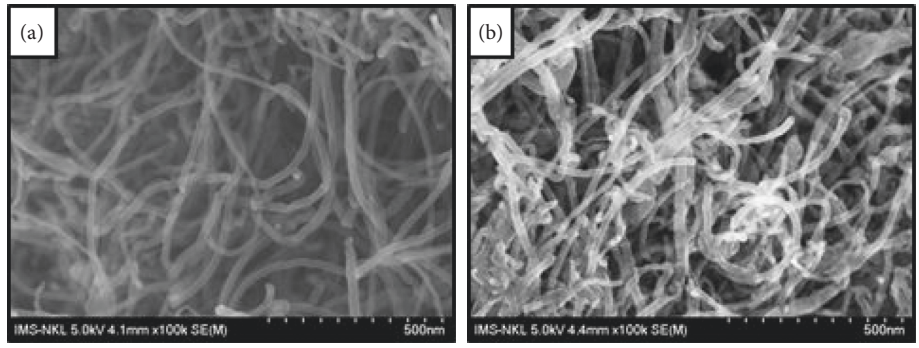

Figure 9: SEM images of bare CNTs (a) and surface-modified CNTs (b).

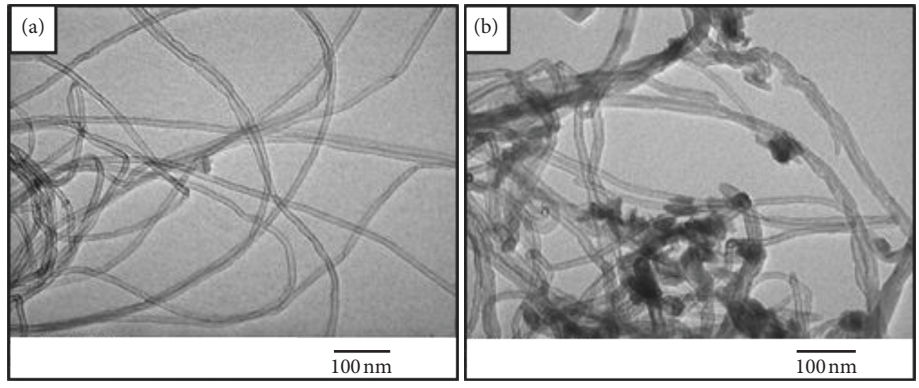

Figure 10: TEM images of bare CNTs (a) and surface-modified CNTs (b).

concentrates on the catalyst particles inside the tube (Figure 12(a)). A low concentration of oxygen and aluminium on the catalyst particles infers two points: (i) Fe_2O_3 might be reduced to Fe and (ii) Fe atoms are separated from the Al_2O_3 substrate during the growth of CNTs. This indicates that the growth mechanism might be tip-growth (Figure 13) [45].

The overlap of the STEM-EDS mapping of iron and oxygen (Figure 14) shows that there is no significant increase of oxygen signals at the iron positions. This partly proves that the particles inside the tubes observed on the STEM image of CNTs are iron nanoparticles, not iron oxides.

The SAED and FFT measurements performed on HR-TEM device are used to determine the distance between atomic planes (Figure 15). The measured values perfectly match the theoretical values of lattice parameters of α-Fe as shown in Table 1 reflecting the reduction of Fe_2O_3 to α-Fe during the synthesis of CNTs. Theoretically, Fe_2O_3 is

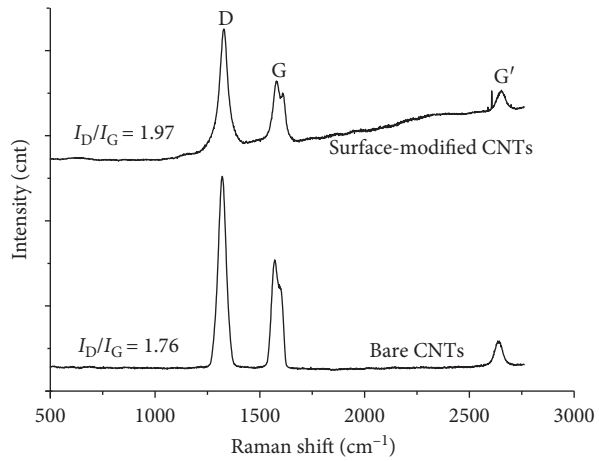

Figure 11: Raman spectra of bare CNTs and surface-modified CNTs.

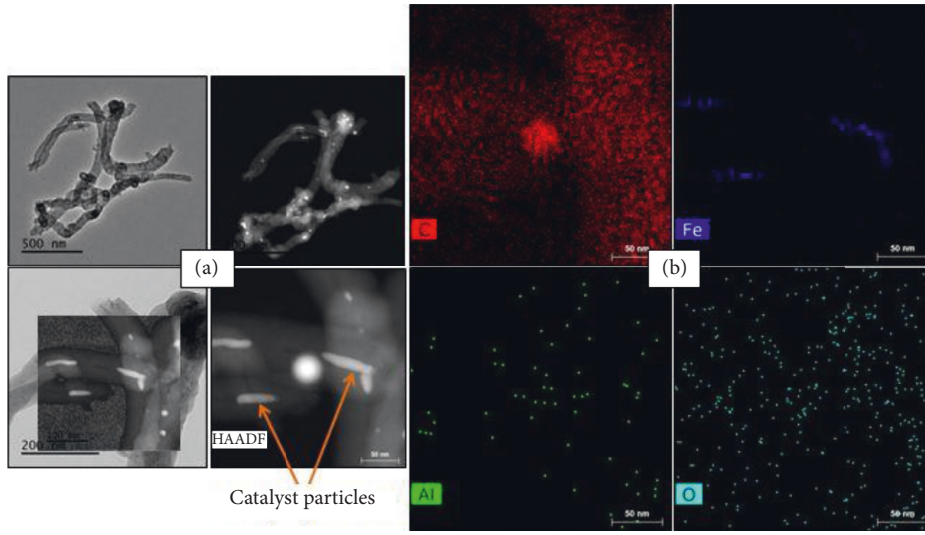

Figure 12: STEM-HAADF (a) and STEM-EDS (b) studies performed on the CNT sample.

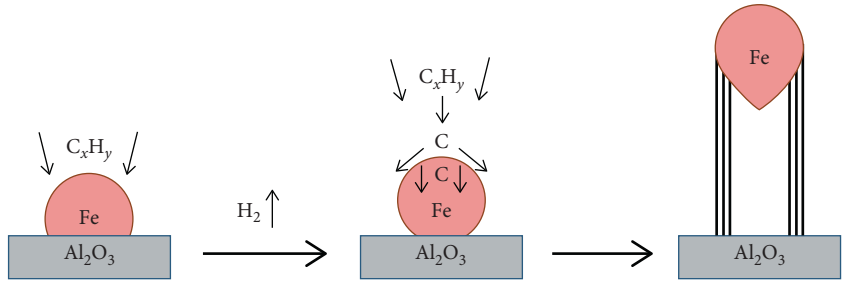

Figure 13: Tip-growth mechanism of CNTs synthesis.

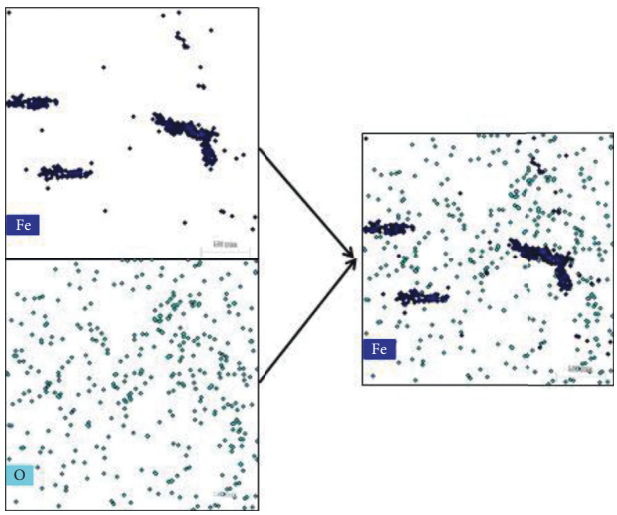

Figure 14: Overlap of the STEM-EDS mapping of Fe and O.

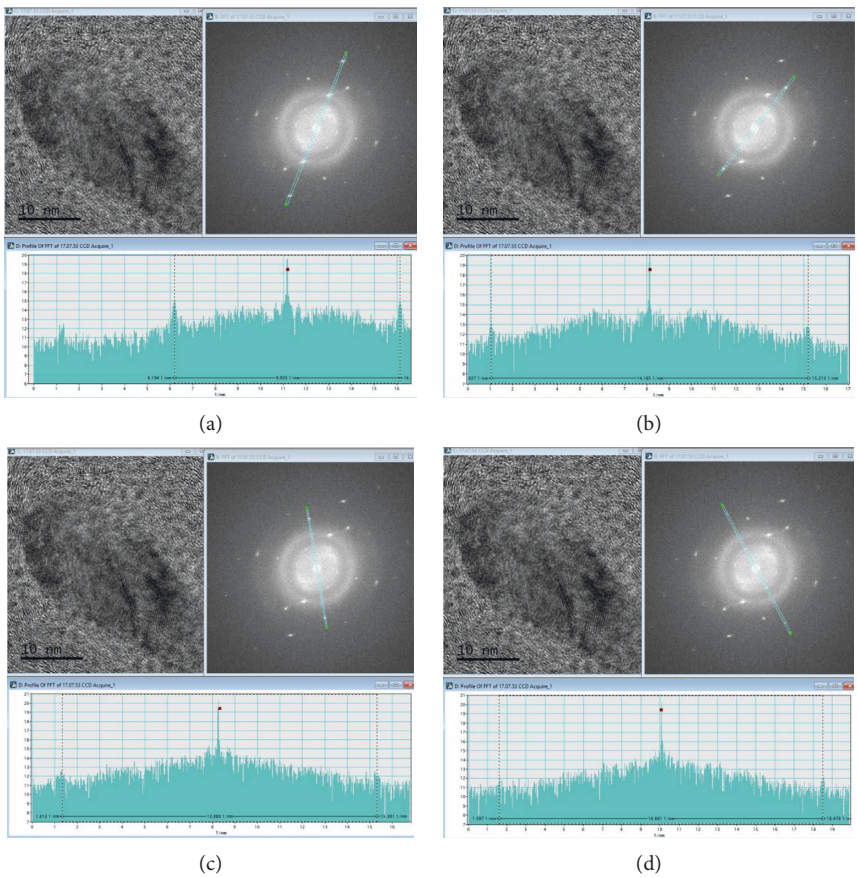

(a) (b)

(c) (d)

Figure 15: Continued.

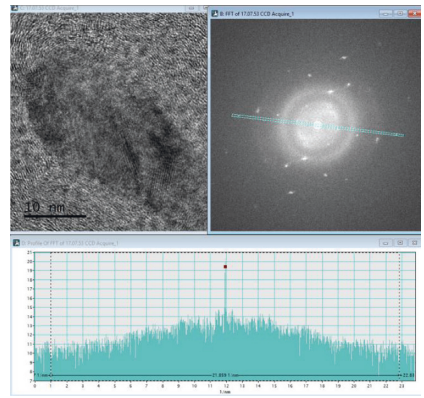

(e)

Figure 15: SAED and FFT measurements on a catalyst particle. (a) $d_1 = 2.013$ Å $\longrightarrow$ (110). (b) $d_2 = 1.410$ Å $\longrightarrow$ (200). (c) $d_3 = 1.429$ Å $\longrightarrow$ (200). (d) $d_4 = 1.185$ Å $\longrightarrow$ (211). (e) $d_5 = 0.915$ Å $\longrightarrow$ (310).

Table 1: Lattice parameters of α-Fe (JCPDS card files no. 6–0696).

No.	h	k	l	d (Å)
1	1	1	0	2.02657
2	2	0	0	1.43300
3	2	1	1	1.17004
4	3	1	0	0.90631

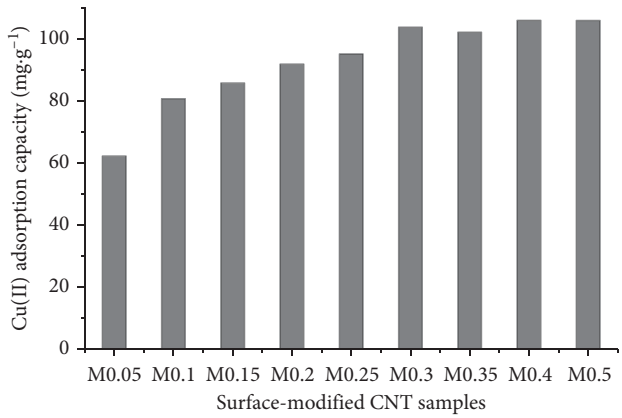

Figure 16: Effect of $KMnO_4$ concentration on Cu(II) adsorption capacity of surface-modified CNTs.

completely reduced to Fe by C at the temperature higher than 565°C or by H_2 at the temperature equal to 425°C. Hence, the reduction of the precatalyst could completely take place at the growth temperature (800°C) by C and H_2 formed from the decomposition of LPG.

In conclusion, the growth of CNTs still takes place on the metal nanoparticle catalyst. Main reactions suggested during the synthesis of CNTs are as follows:

$$2C_xH_{y(g)} \longrightarrow 2xC_{(g)} + yH_{2(g)} \quad (2)$$

$$Fe_2O_{3(\text{nanoscale})}/Al_2O_{3(s)} + C_{(s)}\left(\text{or } H_{2(g)}\right) \longrightarrow Fe_{(\text{nanoscale})}/Al_2O_{3(s)} + CO_{2(g)}\left(\text{or } H_2O_{(g)}\right) \quad (3)$$

$$C_{(g)} + Fe_{(\text{nanoscale})}/Al_2O_{3(s)} \longrightarrow Fe_3C_{(s)}/Al_2O_{3(s)} \quad (4)$$

$$Fe_3C_{(s)}/Al_2O_{3(s)} \longrightarrow CNTs - Fe/Al_2O_{3(s)} \quad (5)$$

3.3. Cu(II) Adsorption onto Surface-Modified CNTs

3.3.1. Surface Modification of CNTs

(1) Effect of $KMnO_4$ Concentration. The Cu(II) adsorption capacity of the CNTs increases gradually from 62.1 to 103.7 mg·g^{-1} with the increase of $KMnO_4$ concentration from 0.05 to 0.3 M and then remains practically stable around 103 mg·g^{-1} (Figure 16). This is because $KMnO_4$ increases the amount of oxygen-containing groups (–OH, –C=O and–COOH) on the surface of CNTs and thus promotes Cu(II) adsorption. Unlike surface-modified CNTs, bare CNTs exhibit much lower Cu(II) adsorption capacity (7.6 mg·g^{-1}). This indicates the crucial role of CNTs modification when CNTs are used in metal adsorption.

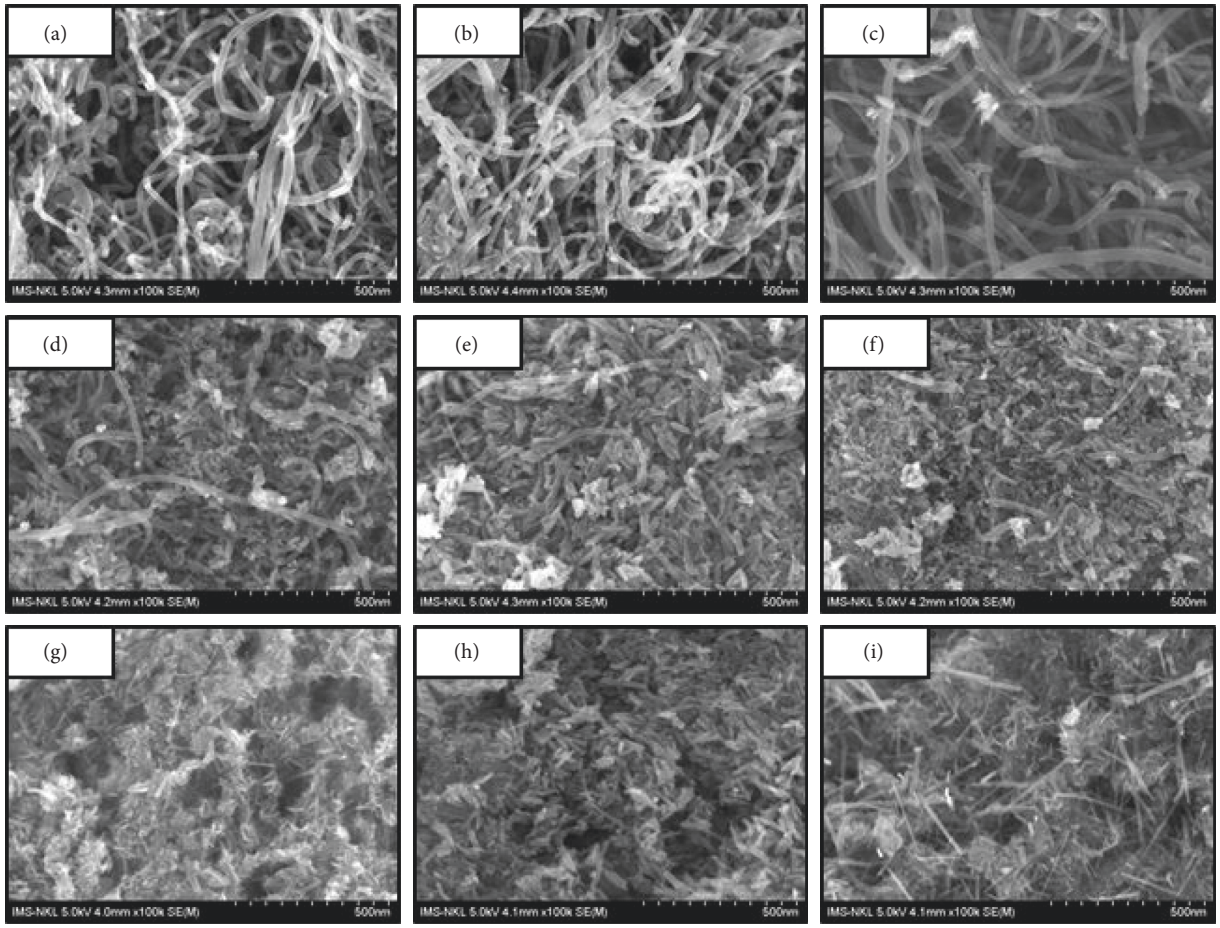

Figure 17: SEM images of surface-modified CNTs prepared with different $KMnO_4$ concentrations. (a) M0.05. (b) M0.10. (c) M0.15. (d) M0.20. (e) M0.25. (f) M0.30. (g) M0.35. (h) M0.40. (i) M0.50.

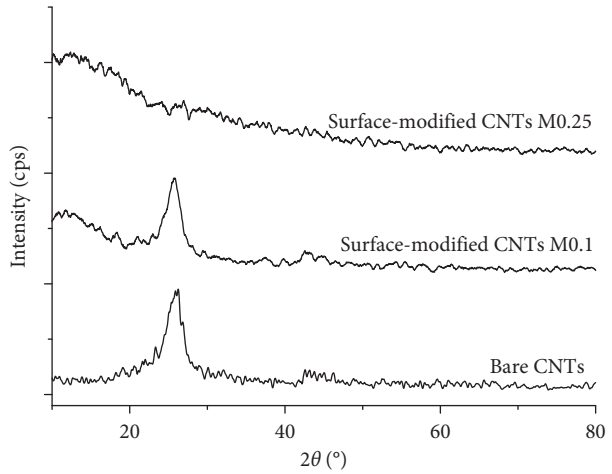

Figure 18: XRD patterns of bare CNT and surface-modified CNT (M0.1 and M0.25) samples.

The morphology of the surface-modified CNTs samples indicates that $KMnO_4$ with higher concentration destroys the tubes causing the tubes to break down to shorter ones (Figure 17). The tubes break considerably when the concentration of $KMnO_4$ reaches 0.2 M and beyond.

The XRD patterns of bare CNT and surface-modified CNT samples (M0.1 and M0.25) (Figure 18) show that when using 0.25 M $KMnO_4$, the crystal phase of carbon disappears and the material becomes amorphous. For the bare CNT and $KMnO_4$-M0.1-modified sample, the characteristic diffraction

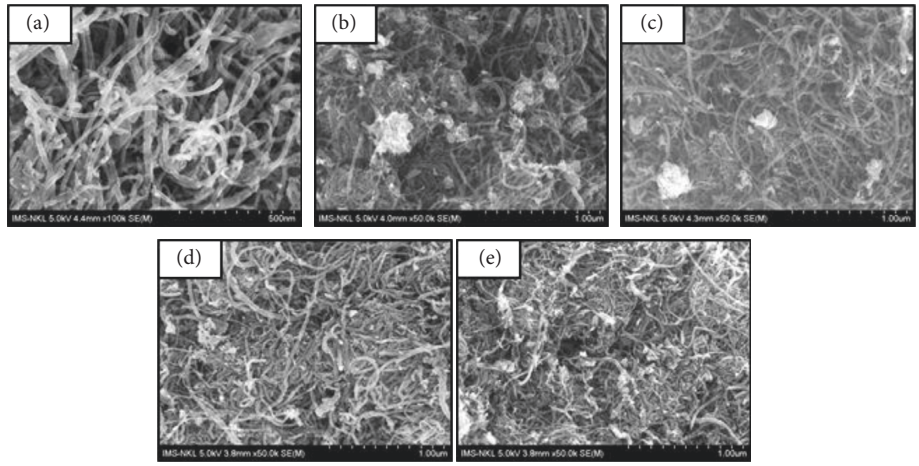

Figure 19: SEM images of surface-modified CNTs prepared at different modification temperatures. (a) M40. (b) M50. (c) M60. (d) M70. (e) M80.

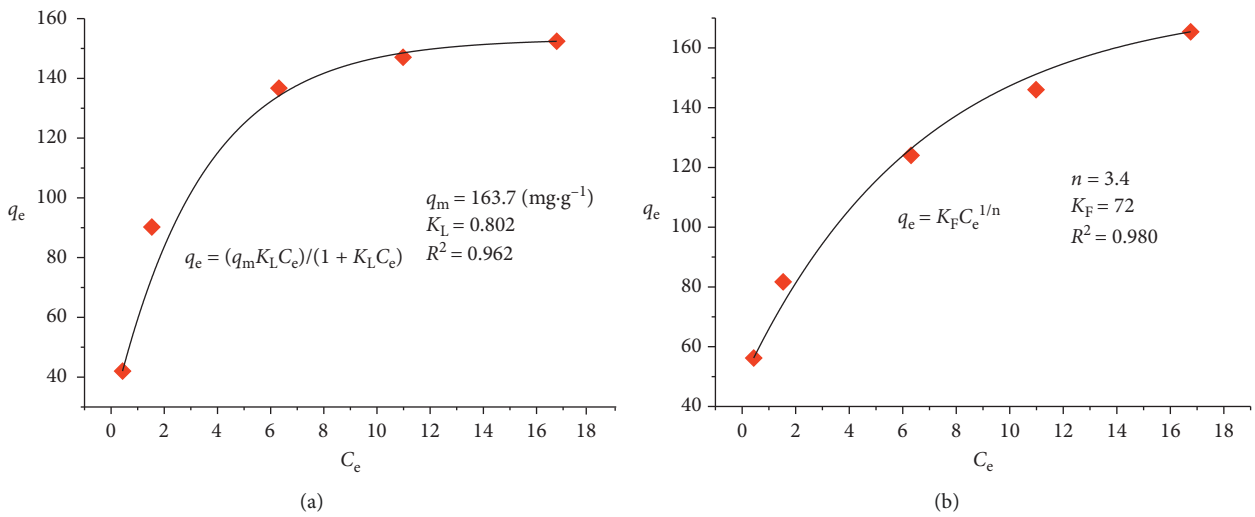

Figure 20: Langmuir (a) and Freundlich (b) isotherm studies on Cu(II) adsorption.

peak of the graphite phase appears at 2θ of 26.22° corresponding to the (002) plane (JCPDS card files, no. 41–1487).

In conclusion, with the concentration of $KMnO_4$ from 0.2 to 0.5 M, the CNT structure collapses completely and the obtained materials change into amorphous carbon. Therefore, the most suitable concentration of $KMnO_4$ should be at 0.1 M, which is consistent with what reported by Slobodian et al. [46] when they oxidize the CNTs network embedded in elastic polyurethane. However, Zhang et al. [47] use the 0.313 M·$KMnO_4$ solution to modify CNTs.

(2) Effect of Modification Temperature and Time. The range of modification temperature was from 40 to 80°C. Although the Cu(II) adsorption capacity of surface-modified CNTs is high (around 102 mg·g^{-1}) in the temperature range from 50 to 80°C, most tubes break and the number of very short tubes increases with temperature (Figure 19). At 40°C, the material exhibits relatively high Cu(II) adsorption capacity (80.8 mg·g^{-1}) and the tube length remains unaltered. The modification of CNTs was carried out for a period from 0.5 to 5 hours under ultrasound. The material modified with the 0.1 M·$KMnO_4$ concentration at 40°C for 2 to 5 hours exhibits unvaried Cu(II) adsorption capacity at around 81 mg·g^{-1}. Therefore, the 2-hour modification under ultrasound is suitable for the obtained CNTs.

3.3.2. Adsorption Isotherm Study. The Langmuir and Freundlich isotherm models [32, 48] were used to evaluate the adsorption with nonlinear equations as follows:

$$q_e = \frac{q_m K_L C_e}{1 + K_L C_e}, \quad (6)$$

$$q_e = K_F C_e^{1/n}, \quad (7)$$

where C_e is the equilibrium concentration of Cu(II) in the solution after adsorption; q_e is the Cu(II) adsorption capacity of modified CNTs calculated from equation (1); q_m is

Table 2: Isotherm parameters calculated from the Langmuir model of Cu(II) adsorption onto many kinds of surface-modified CNTs.

Sorbents	q_m (mg·g^{-1})	R^2	References
CNTs ultrasonically stirred in $KMnO_4$ and H_2SO_4	163.7	0.995	The present study
CNTs refluxed in the solution of HNO_3 and H_2SO_4 at 80°C for 48 h	29.69	0.980	[22]
CNTs refluxed in 65% HNO_3 at 120°C for 48 h	200	0.998	[23]
MWCNTs ultrasonically stirred in 3 M HNO_3 for 24 h	3.439	0.932	[24]
CNTs refluxed in concentrated HNO_3 for 1 h at 140°C	28.49	0.991	[25]
MWCNTs ultrasonically suspended in 3 M HNO_3 for 30 min and then stirred at 110°C for 48 h	53	0.994	[26]
CNTs ultrasonically immersed in 65% HNO_3 for 30 min and then stirred for 3 h at 298 K	13.87	0.980	[27]
CNTs ultrasonically immersed in 60% NaClO for 30 min and then stirred for 3 h at 358 K	47.39	0.987	[27]
CNTs ultrasonically dispersed in 23% HCl and then stirred on a hot plate at 175°C–200°C for 3 h	6.235	0.973	[28]

the maximum Cu(II) adsorption capacity; K_L is the Langmuir constant which is related to the strength of adsorption; and K_F and n are the Freundlich constants [48].

Figure 20 illustrates the nonlinear correlation between q_e and C_e corresponding to Langmuir and Freundlich isotherm models. The determination coefficient for the Langmuir model ($R^2 = 0.962$) is similar to that for the Freundlich model ($R^2 = 0.980$). This indicates that the adsorption is in the monolayer form with the multienergy surface. High determination coefficients imply that 97-98% of the variability of the dependent variable accounts for the equilibrium capacity.

The maximum Cu(II) adsorption capacity (q_m) calculated from the Langmuir nonlinear equation is 163.7 mg·g^{-1}. This indicates that Cu(II) adsorption onto modified CNTs takes place favorably and irreversibly, and the modified CNTs are a good adsorbent. The maximum Cu(II) adsorption capacity of our material is much higher than that of other modified CNTs (Table 2).

4. Conclusions

The CNTs were successfully synthesized from LPG using the CVD method without an initial H_2 flow. The characterization of the obtained CNTs confirms that the purity of the product is about 91.2% (w/w) of hexagonal graphite. The tubes have a multiwalled structure, and they are long, less-defective with an internal and external tube diameter of around 15 and 50 nm. The BET surface area of the obtained CNTs is 134 m^2·g^{-1}. The tip-growth mechanism of CNT formation is suggested. The precatalyst in the form of iron oxide is reduced to iron using hydrogen and carbon formed from the decomposition of hydrocarbon. The synthesized CNTs were surface-modified with $KMnO_4$, and the obtained material exhibits high Cu(II) maximum adsorption capacity at 163.7 mg·g^{-1}.

Data Availability

The data used to support the findings of this study are available from the corresponding author upon request.

Conflicts of Interest

The authors declare that they have no conflicts of interest.

References

[1] S. Iijima, "Helical microtubules of graphitic carbon," *Nature*, vol. 354, no. 6348, pp. 56–58, 1991.

[2] T. Guo, P. Nikolaev, A. G. Rinzler, D. Tomanek, D. T. Colbert, and R. E. Smalley, "Self-assembly of tubular fullerenes," *Journal of Physical Chemistry*, vol. 99, no. 27, pp. 10694–10697, 1995.

[3] M. Endo, K. Takeuchi, S. Igarashi, K. Kobori, M. Shiraishi, and H. W. Kroto, "The production and structure of pyrolytic carbon nanotubes (PCNTs)," *Journal of Physics and Chemistry of Solids*, vol. 54, no. 12, pp. 1841–1848, 1993.

[4] N. Yahya, *Carbon and Oxide Nanostructures: Synthesis, Characterisation and Applications*, Springer Science & Business Media, Berlin, Germany, 2011.

[5] S.-P. Chai, W.-M. Yeoh, K.-Y. Lee, and A. R. Mohamed, "Investigations on the effects of CoO_x to MoO_x ratio and CoO_x–MoO_x loading on methane decomposition into carbon nanotubes," *Journal of Alloys and Compounds*, vol. 488, no. 1, pp. 294–299, 2009.

[6] M. H. Khedr, K. S. A. Halim, and N. K. Soliman, "Effect of temperature on the kinetics of acetylene decomposition over reduced iron oxide catalyst for the production of carbon nanotubes," *Applied Surface Science*, vol. 255, no. 5, pp. 2375–2381, 2008.

[7] P. Singjai, S. Changsarn, and S. Thongtem, "Electrical resistivity of bulk multi-walled carbon nanotubes synthesized by an infusion chemical vapor deposition method," *Materials Science and Engineering: A*, vol. 443, no. 1-2, pp. 42–46, 2007.

[8] B. Kitiyanan, W. E. Alvarez, J. H. Harwell, and D. E. Resasco, "Controlled production of single-wall carbon nanotubes by catalytic decomposition of CO on bimetallic Co–Mo catalysts," *Chemical Physics Letters*, vol. 317, no. 3-5, pp. 497–503, 2000.

[9] P. Ndungu, Z. G. Godongwana, L. F. Petrik, A. Nechaev, S. Liao, and V. Linkov, "Synthesis of carbon nanostructured materials using LPG," *Microporous and Mesoporous Materials*, vol. 116, no. 1–3, pp. 593–600, 2008.

[10] A. Songsasen and P. Pairgreethaves, "Preparation of carbon nanotubes by nickel catalyzed decomposition of liquefied

petroleum gas (LPG)," *Kasetsart Journal—Natural Science*, vol. 35, pp. 354–359, 2001.

[11] J. M. Zhou, G. D. Lin, and H. B. Zhang, "Efficient growth of MWCNTs from decomposition of liquefied petroleum gas on a $Ni_xMg_{1-x}O$ catalyst," *Catalysis Communications*, vol. 10, no. 14, pp. 1944–1947, 2009.

[12] M. A. Pasha, A. Shafiekhani, and M. A. Vesaghi, "Hot filament CVD of Fe-Cr catalyst for thermal CVD carbon nanotube growth from liquid petroleum gas," *Applied Surface Science*, vol. 256, no. 5, pp. 1365–1371, 2009.

[13] M. S. Dresselhaus, G. Dresselhaus, and P. Avouris, *Carbon Nanotubes: Synthesis, Structure, Properties, and Applications*, Springer-Verlag, Berlin, Germany, 2001.

[14] C. Emmenegger, P. Mauron, A. Züttel et al., "Carbon nanotube synthesized on metallic substrates," *Applied Surface Science*, vol. 162-163, no. 163, pp. 452–456, 2000.

[15] C. L. Cheung, A. Kurtz, H. Park, and C. M. Lieber, "Diameter-controlled synthesis of carbon nanotubes," *Journal of Physical Chemistry B*, vol. 106, no. 10, pp. 2429–2433, 2002.

[16] U. C. Chung, "Effect of H_2 on formation behavior of carbon nanotubes," *Bulletin of the Korean Chemical Society*, vol. 25, no. 10, pp. 1521–1524, 2004.

[17] A. Firouzi, S. Sobri, F. M. Yasin, and F. L. R. Ahmadun, "Synthesis of carbon nanotubes by chemical vapor deposition and their application for CO_2 and CH_4 detection," *International Proceedings of Chemical, Biological and Environmental Engineering*, vol. 2, pp. 169–172, 2011.

[18] Y. S. Shin, J. Y. Hong, D. H. Ryu et al., "The role of H_2 in the growth of carbon nanotubes on an AAO template," *Journal of the Korean Physical Society*, vol. 50, no. 4, pp. 1068–1072, 2007.

[19] L. Zhang, L. Balzano, and D. E. Resasco, "Single-walled carbon nanotubes of controlled diameter and bundle size and their field emission properties," *Journal of Physical Chemistry B*, vol. 109, no. 30, pp. 14375–14381, 2005.

[20] Z. Niu and Y. Fang, "Effect of temperature for synthesizing single-walled carbon nanotubes by catalytic chemical vapor deposition over Mo-Co-MgO catalyst," *Materials Research Bulletin*, vol. 43, pp. 1393–1400, 2007.

[21] United State Environmental Protection Agency (EPA), Washington DC 2008 Document no. EPA 816-F-08-018.

[22] J. Wang, Z. Li, S. Li et al., "Adsorption of Cu(II) on oxidized multi-walled carbon nanotubes in the presence of hydroxylated and carboxylated fullerenes," *PLoS One*, vol. 8, no. 8, Article ID e72475, 2013.

[23] S. Sobhanardakani, R. Zandipak, and M. Cheraghi, "Adsorption of Cu^{2+} ions from aqueous solutions using oxidized multi-walled carbon nanotubes," *Avicenna Journal of Environmental Health Engineering*, vol. 2, no. 1, 2015.

[24] G. Sheng, J. Li, D. Shao et al., "Adsorption of copper(II) on multiwalled carbon nanotubes in the absence and presence of humic or fulvic acids," *Journal of Hazardous Materials*, vol. 178, no. 1–3, pp. 333–340, 2010.

[25] Y.-H. Li, Z. Luan, X. Xiao et al., "Removal of Cu^{2+} ions from aqueous solutions by carbon nanotubes," *Adsorption Science & Technology*, vol. 21, no. 5, 2003.

[26] P. E. Namin, "Adsorption of copper, cobalt and manganese ions from aqueous solutions using oxidized multi-walled carbon nanotubes," *Environment Protection Engineering*, vol. 42, no. 4, 2016.

[27] C.-H. Wu, "Studies of the equilibrium and thermodynamics of the adsorption of Cu^{2+} onto as-produced and modified carbon nanotubes," *Journal of Colloid and Interface Science*, vol. 311, no. 2, pp. 338–346, 2007.

[28] S. Rosenzweig, G. A. Sorial, E. Sahle-Demessie, and J. Mack, "Effect of acid and alcohol network forces within functionalized multiwall carbon nanotubes bundles on adsorption of copper(II) species," *Chemosphere*, vol. 90, no. 2, pp. 395–402, 2013.

[29] E. M. I. Elsehly, N. G. Chechenin, A. V. Makunin, E. A. Vorobyeva, and H. A. Motaweh, "Oxidized carbon nanotubes filters for iron removal from aqueous solutions," *International Journal of New Technologies in Science and Engineering*, vol. 2, pp. 14–18, 2015.

[30] A. A. Moosa, A. M. Ridha, and I. N. Abdullha, "Chromium ions removal from wastewater using carbon nanotubes," *International Journal of Innovative Research in Science, Engineering and Technology*, vol. 4, pp. 275–282, 2015.

[31] X. Peng, J. Jia, and Z. Luan, "Oxidized carbon nanotubes for simultaneous removal of endrin and Cd(II) from water and their separation from water," *Journal of Chemical Technology & Biotechnology*, vol. 84, no. 2, pp. 275–278, 2009.

[32] A. Stafiej and K. Pyrzynska, "Adsorption of heavy metal ions with carbon nanotubes," *Separation and Purification Technology*, vol. 58, pp. 49–52, 2007.

[33] V. Datsyuk, M. Kalyva, K. Papagelis et al., "Chemical oxidation of multiwalled carbon nanotubes," *Carbon*, vol. 46, no. 6, pp. 833–840, 2008.

[34] S.-M. Yoon, S. J. Kim, H.-J. Shin et al., "Selective oxidation on metallic carbon nanotubes by halogen oxoanions," *Journal of the American Chemical Society*, vol. 130, no. 8, pp. 2610–2616, 2008.

[35] Q. Zehua and W. Guojian, "Effective chemical oxidation on the structure of multiwalled carbon nanotubes," *Journal of Nanoscience and Nanotechnology*, vol. 12, no. 1, pp. 105–111, 2012.

[36] J. Zhang, J. Li, J. Cao, and Y. Qian, "Synthesis and characterization of larger diameter carbon nanotubes from catalytic pyrolysis of polypropylene," *Materials Letters*, vol. 62, no. 12-13, pp. 1839–1842, 2008.

[37] A. Cao, C. Xu, J. Liand, D. Wu, and B. Wei, "X-ray diffraction characterization on the alignment degree of carbon nanotubes," *Chemical Physics Letters*, vol. 344, pp. 13–17, 2011.

[38] S. Gopalakrishnan and S. Narendar, "Wave propagation in nanostructures," in *Chapter 8: Wave Propagation in Multiwalled Carbon Nanotubes*, pp. 215–237, Springer International Publishing Switzerland, Berlin, Germany, 2013.

[39] X. M. Sui, S. Giordani, M. Prato, and H. Wagner, "Effect of carbon nanotube surface modification on dispersion and structural properties of electrospun fibers:," *Applied Physics Letters*, vol. 95, no. 1–3, article 233113, 2009.

[40] Y. H. Li, Z. C. Di, Z. K. Luan et al., "Removal of heavy metals from aqueous solution by carbon nanotubes: adsorption equilibrium and kinetics," *Journal of Environmental Sciences*, vol. 16, no. 2, pp. 208–211, 2004.

[41] R. T. K. Baker, "Catalytic growth of carbon filaments," *Carbon*, vol. 27, no. 3, pp. 315–323, 1989.

[42] Y. Yan, J. Miao, Z. Yang et al., "Carbon nanotube catalysts: recent advances in synthesis, characterization and applications," *Chemical Society Reviews*, vol. 44, no. 10, pp. 3295–3346, 2015.

[43] M. Kumar and Y. Ando, "Chemical vapor deposition of carbon nanotubes: a review on growth mechanism and mass production," *Journal of Nanoscience and Nanotechnology*, vol. 10, no. 6, pp. 3739–3758, 2010.

[44] J.-P. Tessonnier and D. S. Su, "Recent progress on the growth mechanism of carbon nanotubes: a review," *ChemSusChem*, vol. 4, no. 7, pp. 824–847, 2011.

[45] N. M. Rodriguez, "A review of catalytically grown carbon nanofibers," *Journal of Materials Research*, vol. 8, no. 12, pp. 3233–3250, 1993.

[46] P. Slobodian, P. Riha, R. Olejnik, U. Cvelbar, and P. Saha, "Enhancing effect of $KMnO_4$ oxidation of carbon nanotubes network embedded in elastic polyurethane on overall electro-mechanical properties of composite," *Composites Science and Technology*, vol. 81, pp. 54–60, 2013.

[47] N. Zhang, J. Xie, and V. K. Varadan, "Functionalization of carbon nanotubes by potassium permanganate assisted with phase transfer catalyst," *Smart Materials and Structures*, vol. 11, pp. 962–965, 2014.

[48] S. Srivastava, "Sorption of divalent metal ions from aqueous solution by oxidized carbon nanotubes and nanocages: a review," *Advanced Materials Letters*, vol. 4, no. 1, pp. 2–8, 2013.